

First Demonstration and Physical Insights into Time-dependent Breakdown of Graphene Channel and Interconnects

Abhishek Mishra^{1,2}, Adil Meersha¹, N.K. Kranthi¹, Kruti Trivedi¹, Harsha B. Variar¹,
N S Veenadhari Bellamkonda¹, Srinivasan Raghavan² and Mayank Shrivastava¹

¹Department of Electronic Systems Engineering, ²Centre for Nano Science and Engineering
Indian Institute of Science, Bangalore, India, Email: mayank@iisc.ac.in

Abstract—A prolonged operation of Graphene FET and interconnects mandate the assessment of temporal evolution of degradation of the material. Contrary to bulk semiconductors, which break only above a critical field, the time-dependent degradation and consequent failure of graphene has been discovered, which precludes the existence of failure threshold and manifests as a potential defect-assisted aging issue for graphene and other 2D material-based devices. Unlike catastrophic failures, which are triggered during redistribution of excess energy, the role of reaction kinetics (time) in inflicting defect-by-defect damage to graphene channel is revealed. Time-evolution of defects in graphene channel while exploring possible pathways through which heat dissipates across the device has been studied on-the-fly using an integrated micro-Raman setup. The role of metal-graphene interface and the substrate in removing excess heat from graphene channel is discussed, while emphasizing the need for *sp*-hybridized carbon atoms at metal-graphene interface for reliable, long-term operation of graphene-based devices.

Index Terms—Aging, Defects, Graphene, Time-dependent failure

I. INTRODUCTION

VERY high carrier mobility and thermal conductivity of graphene has made it a promising material for THz [1], [2], [3] and interconnect [4] applications. While rapid efforts are being made for improving and benchmarking the graphene technology [1], reliability of material [5], [6] under high electric-field or high current need special attention to understand possible failure / breakdown threshold. Contrary to much investigated bulk semiconductors, where the device failure is either related to self-heating under high currents or avalanche breakdown under high electric-fields, graphene failure in this work is discovered to be defect assisted and time-dependent in nature. The reliability assessment for a device is generally done in a framework of electric field and time. At high electric fields and temperature, the device reliability is generally evaluated against *external* catastrophic events like electrostatic discharge or electrical over stress. These events happen at the time scales in the range of nano-seconds to micro-seconds, and are consequent of inelastic scattering-assisted redistribution of excess energy in the system [7]. Failure of the device, in such a case, happens via an energy route. Under normal operating conditions, the devices are expected to operate for a longer duration, while sustaining low electric fields. For a comprehensive understanding of the

reliability and robust operation of the device, it is imperative that the reliability assessment is also done against low electric fields, while operating the device for longer duration. In other words, it is important to evaluate the reliability of the device against *internal* factors and understand the mechanism behind breakdown at low electric fields. In this work, we give a phenomenological description of defect-assisted electro-thermal time-dependent breakdown of graphene channel, while using nano-second to long-term electrical stress with on-the-fly micro-Raman investigations of graphene channel under stress. For a comprehensive understanding of reliability, the breakdown behaviour is further investigated while considering the efficiency of two dominant heat sinks in the device - metal contacts and substrate. The rest of the paper is organized as follows: section II discusses experimental techniques used to process devices and perform measurements to capture the evolution of defects with time and electric field. The mechanism behind site-specific defect-by-defect failure in time domain and field domain is discussed in section III. Section IV discusses the dependence of breakdown behaviour on the efficiency of various heat sinks. The overall work is concluded in section V.

II. DEVICE FABRICATION AND CHARACTERIZATION

Devices used in the work were fabricated using bottom-up approach. In brief, CVD-grown graphene was first transferred to SiO₂/Si stack, followed by channel definition and contact patterning using O₂ plasma and e-beam lithography, respectively. Before metallization of contacts, defects were deterministically introduced through controlled exposure to an electron beam [1]. Failure investigation begins with infliction of a series of controlled defects by two different approaches – (1) time-dependent breakdown, by applying moderate-fields for elongated durations, until partial/complete breakdown is achieved and (2) field-dependent breakdown, by applying high-field for few nano-seconds and increasing the magnitude until breakdown. In both the methods, the device resistance and defect density are closely monitored using integrated on-the-fly micro-Raman spectroscopy setup to capture the evolution of defects with time and electric-field (figure 1). Assuming low-defect density (distance between defects > 10 nm), the defect density ($n_D(cm^{-2})$) can be approximated as

$\frac{(1.8 \pm 0.5) \times 10^{22}}{\lambda_L^4} \frac{I_D}{I_G}$, where λ_L is the wavelength in nano metres and $\frac{I_D}{I_G}$ corresponds to ratio of D-peak to G-peak in the Raman spectrum. For devices with pristine and defected channels, the expression reveals a defect density of approximately $1.5 \times 10^{10} \text{ cm}^{-2}$ and $11.25 \times 10^{10} \text{ cm}^{-2}$, respectively [8]. Note that the electric-field mentioned henceforth corresponds to the ratio of drain-source voltage and the channel length.

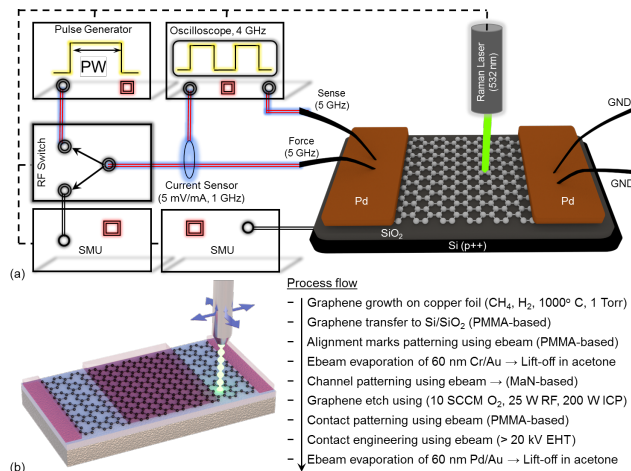


Fig. 1: (a) Electro-optical technique used to capture electrical and Raman signatures of defect evolution in a graphene channel. A transmission line pulse tester (along with inductive current sensor and high frequency oscilloscope) is employed to apply high electric fields for a duration of few nanoseconds, while DC SMUs are used to monitor time-dependent breakdown. A Raman spectrometer (LabRam HR), is used to generate a defect map and quantify the defects after every occurrence of time/field induced defect. Raman maps are acquired with reduced laser power, to avoid any unintentional damage to the material, while defects are captured through a slow scan of 4 seconds at every spot of the device. In case of pulse measurements, the current and voltage data-points are acquired after averaging from 70% to 90% of the transient waveform. (b) Process flow used to fabricate back-gated graphene based-devices. A schematic depicting creation of defects using electron beam is also shown. The controlled exposure enables a lever to tune the density of sp -hybridized states and bring a deterministic change in contact resistance [1].

III. TIME-DEPENDENT FAILURE OF GRAPHENE

Unlike bulk semiconductors or metals, where the device failure is either related to self-heating under high currents or avalanche breakdown under high electric-fields (only in case of semiconductors), 2D materials like graphene can undergo chemical oxidation of carbon atoms. The rate of oxidation of carbon (k) decays exponentially with E_a/T , where E_a is activation energy of the carbon lattice and T is temperature for oxidation [9]. Further, the lattice sites with low activation energy for oxidation are oxidized first, followed by the ones with high activation energy. In order to comprehend the site-specific oxidation, we discuss an important dissimilarity

between crystal structure of state-of-the-art silicon and large area monolayer of graphene. The single crystal silicon used to process devices is grown by Czochralski process, and is generally free of defects. The large area graphene is grown by chemical vapor deposition, wherein catalytic decomposition of methane over copper results in nucleation of graphene grains, which coalesce together to stitch a monolayer of large area graphene. Such a growth mechanism results in formation of boundaries and triple junctions at the mergence of various grains, which constitute defects in CVD-grown graphene. Moreover, the two-dimensional nature of the material and high temperature growth on metal results in formation of wrinkles, folds and voids/vacancies across the sheet of graphene, all of which constitutes defect structures in a CVD grown graphene. Due to existence of various defect structures, a monolayer of CVD grown graphene shows a spatial variation in activation energy for oxidation. Interestingly, it has been observed that unique defect types result in different temperature values at a given electric-field [10], which in-turn imparts temporal and spatial variation to oxidation. The temporal nature of the oxidation is captured in figure 2, where the devices show a series of time-dependent breakdown, before undergoing a complete damage, in a defect-by-defect fashion. The defect-by-defect breakdown can occur either due to time factor (figure 2) or temperature factor (figure 3). It is important to highlight the key difference between breakdown behaviours shown in figure 2 and figure 3. The degradation behaviour captured in figure 2 shows a series of discrete rise in resistance after a constant stress on $1 \text{ V}/\mu\text{m}$ for hundreds of seconds. Contrary to this, the breakdown behaviour shown in figure 3 corresponds to an electric field in excess of $6 \text{ V}/\mu\text{m}$ and a stress duration of 25 ns. Note that the breakdown behaviours shown in figure 2 and 3 happen because of temperature-assisted oxidation of carbon. The breakdown at lower electric fields (figure 2) happens at smaller population of phonons and at lower temperature, while the breakdown at higher electric fields (figure 3) happens at larger population of phonons and at higher temperature. Since population of optical phonons, and hence temperature, increases with electric field, therefore the breakdown behaviour shown in figure 3 happens at a relatively higher temperature than the behaviour shown in figure 2. Consequently, the former breakdown happens due to rapid oxidation of the lattice, while the latter shows slow oxidation of carbon. Hence, it is concluded that the breakdown due to higher electric fields, shown in figure 3, happens primarily due to temperature sufficient to cause early or instantaneous oxidation of carbon lattice. Also, the time factor shown in figure 2 is 10^{11} times longer than the time factor involved in figure 3. The break-down is mediated by time, because a small but non-zero rate of oxidation causes a delayed breakdown. Although crucial to analysis, the temperature profile could not be extracted due to limitation of the measurement system. The results of Raman thermometry published elsewhere shows that the temperature of the lattice could range from 900 K to 1500 K, while dissipating power from 1 mW to 3 mW [11].

In order to further understand the defect-by-defect breakdown behaviour of graphene, we consider two different sets of pathways for oxidation of the lattice. The first pathway,

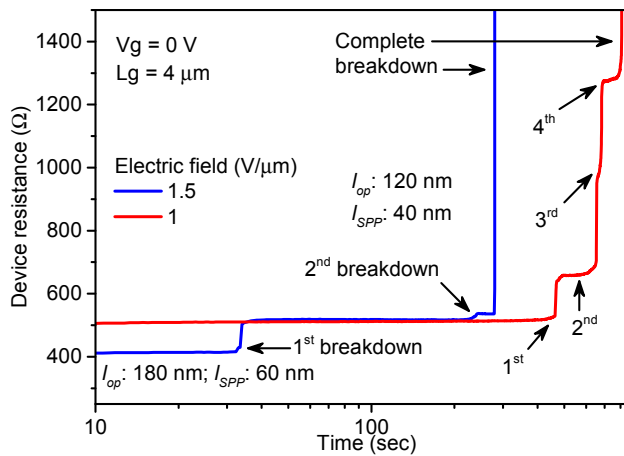


Fig. 2: Signatures of time-evolution of defects. The devices are stressed with constant electric-field (E), until a complete breakdown is achieved. Temporally, abrupt increments in the device resistance are observed at repeated instances, which indicates time-evolution of defects. l_{SPP} and l_{op} are mean free paths for scattering of surface polar phonons ($\hbar\Omega = 60$ meV) and graphene optical phonons ($\hbar\Omega = 180$ meV), respectively. An approximate value of mean free path is calculated using $\hbar\Omega/eE$.

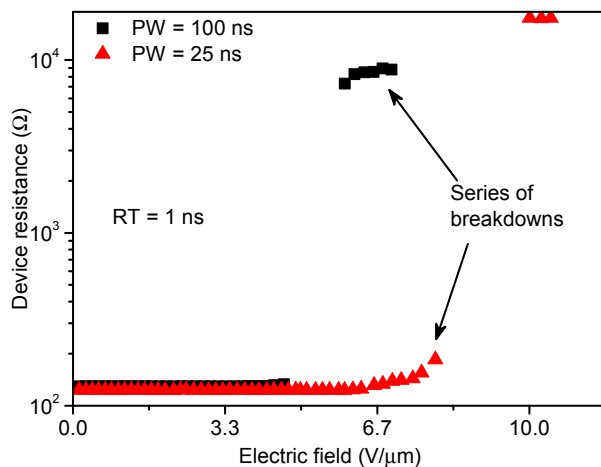


Fig. 3: Evidence of defect-by-defect breakdown captured by injecting nanosecond charge bursts. The gradual increment in the electric-field causes proportional rise in the lattice temperature, due to which defects undergo temperature-specific oxidation. The device shows a series of partial breakdowns before undergoing complete failure.

henceforth referred as intrinsic pathway, corresponds to oxidation of the pristine (defect free) lattice of carbon, which due to involvement of sp^2 hybridized carbon atoms could require high activation energies. The second set of pathways corresponds to oxidation via defect sites. The change in hybridization or vacancies at the defect sites lowers the barrier required for oxidation. This pathway, which initiates oxidation from non-hexagonal arrangement of atoms, is referred as extrinsic route to oxidation. A schematic of the pathways is shown in figure 4. The CVD growth of graphene at high temperatures and

the transfer of monolayer to the target substrate result in formation of various defect structures across the monolayer of graphene. Consequently, the extrinsic route plays a dominant role in oxidation of graphene. Due to limitation of the Raman spectrometer (probe diameter $> 1 \mu\text{m}$) and unavailability of devices on single grains of graphene, the precise defect density for transition from intrinsic to extrinsic pathway, and the critical field required for the oxidation through intrinsic pathway could not be quantified.

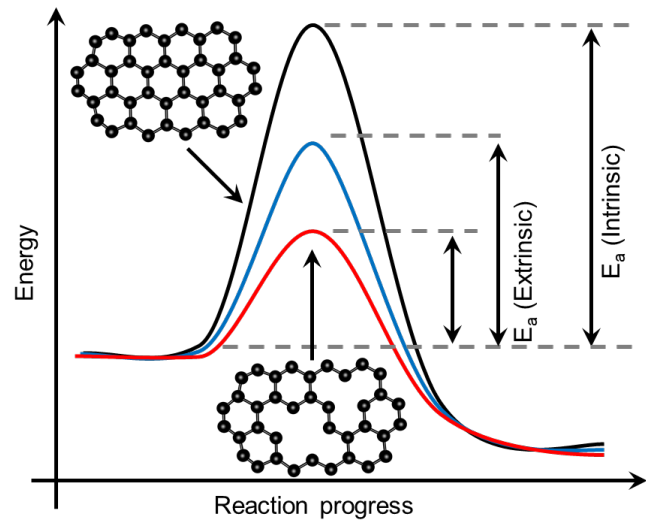


Fig. 4: Schematic describing possible pathways for oxidation of graphene. The activation energy corresponds to a sum of binding energy at the site of oxidation and the energy required for oxidation of carbon. The binding energy, in turn, is smaller for the sites with defects. For an SiO_2 supported graphene, the interiors of grain, or pristine hexagonal network, requires an activation energy of around 1.85 eV for oxidation in dry air, which is sufficiently large compared to thermal energy at room temperature [12].

The site-preference of oxidation is captured through Raman mapping after every occurrence of abrupt increase in resistance during time-stressing of the device at constant electric field (figure 5). Investigation of the Raman map shows increase in D-peak intensity and reduction in the intensity of G-peak. In a hexagonal lattice of carbon atoms, the D-peak signifies a breakdown of symmetry, while G-peak represents hexagonal arrangement of carbon atoms. Hence, increase in D-peak represents creation of more defects, while decrease in G-peak represents removal of carbon due to oxidation at high temperatures. Hence, the time-evolution of defects is a two-step process – (1) excessive scattering and eventual heat dissipation at the defect site and (2) oxidation at the defect site, resulting in emergence of more defects. A cascade of these two processes result in permanent failure of graphene (figure 5 and 6). The breakdown shows interesting time and field dependence. High-field results in early oxidation and breakdown of the channel, while low-field requires longer stress time for oxidation (figure 7). Hence, contrary to bulk semiconductors, where failure threshold is decided by temperature or field

inside local hotspot, the failure of graphene is predominantly dictated by activation energy required to oxidize the lattice site at a given temperature. The time-evolution of defects depict a direct consequence on time-dependent aging of the device, which permanently shifts the device characteristics and lowers the channel performance.

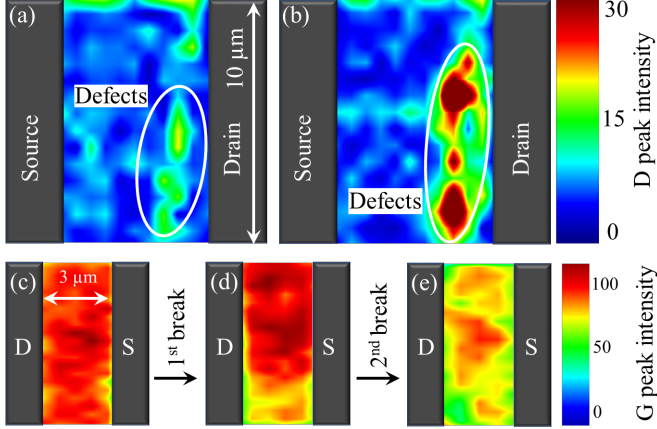


Fig. 5: (a-b) Site preference of oxidation (a) pristine device (b) post-breakdown. The damage occurs primarily around defect site near the drain (hot) contact, which is indicated by increase in intensity of D-peak. This depicts susceptibility of defects towards oxidation. (c-e) Time-evolution of defects at constant electric-field of $1.5 \text{ V}/\mu\text{m}$. G-peak across (c) Pristine device, and (d)-(e) device after 1^{st} and 2^{nd} breakdown, respectively, depicting damage at different time instants. Reduction in the intensity of G-peak indicates gradual oxidation of the graphene channel. The maps were generated by capturing the defect peak at 1350 cm^{-1} and G-peak at 1580 cm^{-1} across the device at different time instants. Simultaneous analysis of change in intensities of G-peak and D-peak indicates scattering-induced rise in temperature at defect site, followed by increase in defect density and eventual oxidation of the lattice of carbon atoms.

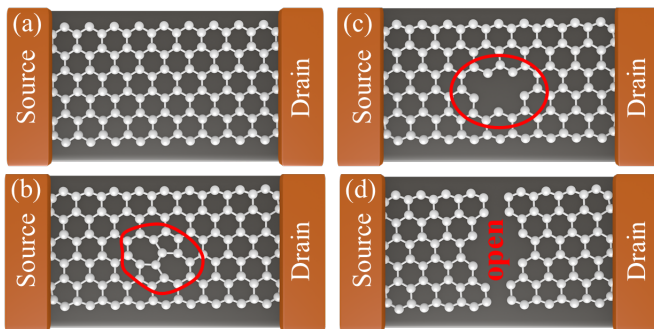


Fig. 6: A pictorial representation of defect-evolution in graphene. (a) pristine lattice of graphene; (b) topological defects (5-7) shown in red; (c) maximum scattering and oxidation happens at the defect site (5-7), resulting in increase in defect density; (d) further increase in time/field causes complete oxidation of the lattice. (c) and (d) constitute time-dependent defect-by-defect breakdown.

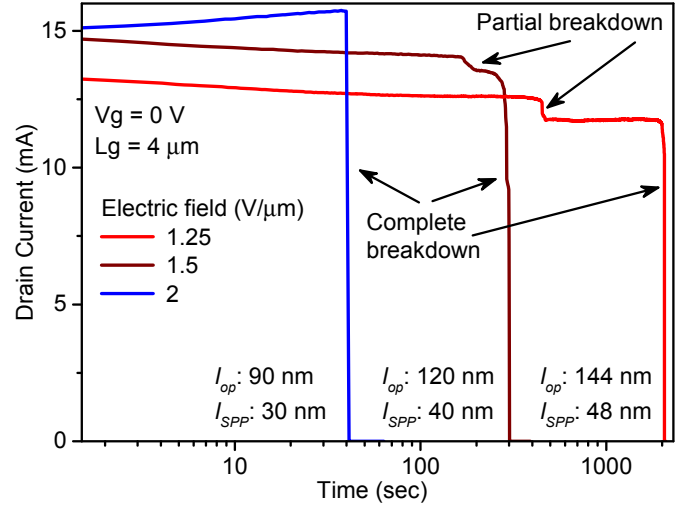


Fig. 7: Field (E) and time dependence of breakdown. The devices are stressed with constant field until permanent failure. Higher (lower) fields result in dense (sparse) distribution of phonons, consequently early (delayed) breakdown. l_{SPP} and l_{op} are mean free paths for scattering of surface polar phonons ($\hbar\Omega = 60 \text{ meV}$) and graphene optical phonons ($\hbar\Omega = 180 \text{ meV}$), respectively. An approximate value of mean free path is calculated using $\hbar\Omega/eE$.

IV. ROLE OF GRAPHENE-METAL/DIELECTRIC INTERFACE

Under high electric-fields, the inelastic collision of hot electrons generates thermal energy, dissipation of which depends on heat removal efficiency of the heat sinks (substrate and metal contacts) next to the hot spot. Consequently, electric-field required for breakdown varies with thermal conductance of the substrate [13] and contact resistance of metal-graphene interface. The dependence of failure on thermal conductance of substrate is shown in figure 8, where, electric field required for breakdown increases with thermal conductance of the substrate. The devices show scaling of current with width and a similar normalized current across all the widths (inset of figure 8a). The field required for breakdown also scales with the width. Since current density is approximately the same across all the widths, scaling of the breakdown field suggests enhancement in cooling of the lattice with increase in width, or thermal conductance of the substrate. Moreover, the rate of degradation of channel decreases with increase in thermal conductance. Both of these observations are attributed to decrease in channel temperature with increase in thermal conductance. The Arrhenius dependence of oxidation of carbon on temperature results in decrease in rate of oxidation with increase in thermal conductance of the device, which in turn decreases the rate of degradation at a particular electric field or temperature.

The dependence of breakdown on metal contacts is more complicated and requires investigation of devices with variation in thermal coupling at metal-graphene interface. The devices used for such an investigation are realized by controlled creation of defects in graphene at metal-graphene interface, which directly changes the transport at the interface and can

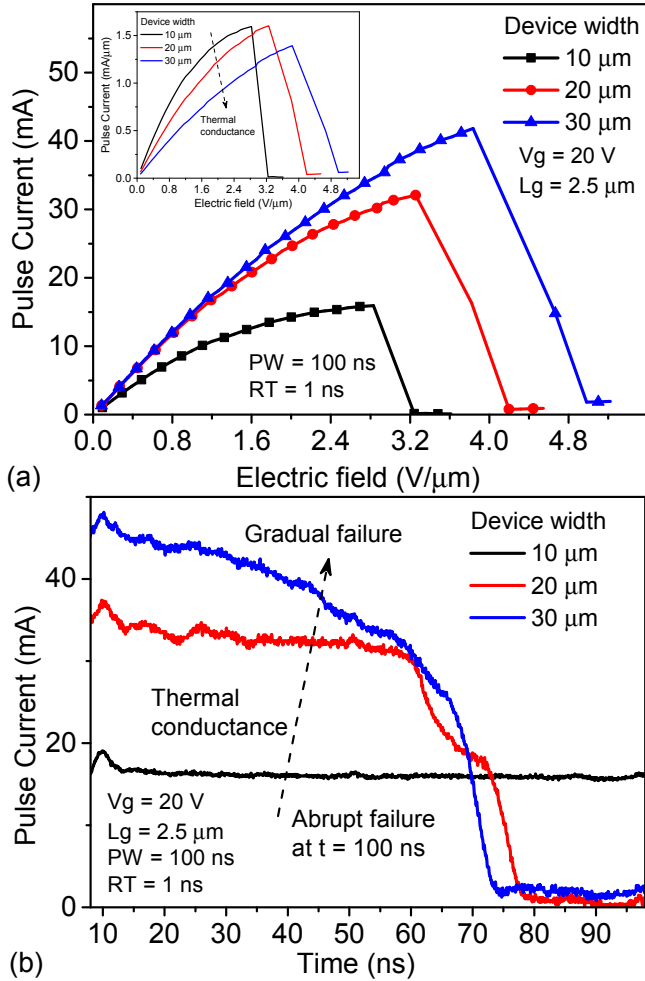


Fig. 8: (a) Dependence of breakdown behavior on device width. Increase in device width improves thermal conduction of heat from graphene to SiO_2/Si , which in turn reduces the population of both graphene optical phonons and surface polar phonons. Consequently, electric field and current required for breakdown scales with device width. Lowering of optical phonons population is also evident from decrease in current saturation with increase in thermal conductance. (b) Channel breakdown becomes increasingly gradual in nature with increased thermal conductance, which is due to reduced channel temperature or phonon population.

be quantified by extraction of contact resistance. Under high-current injection, due to absence of physical metal-graphene bonding and tunneling-based transmission [1], a heavy current crowding [14] and eventual resistive heating manifests across metal-graphene interface. The crowding and resistive heating, in turn, create a phonon bottleneck for transfer of thermal energy from graphene to metal contacts. Such a bottleneck for optical phonons near hot-contact decreases the breakdown voltage (figure 9) and causes breakdown near the contact (figure 10). Contrary to the tunnelling-based metal-graphene interface, the contact engineered by creating *sp*-hybridized defects at the metal-graphene interface improves bonding between metal and graphene, which, in turn, suppresses the

tunnelling component of transmission and improves the exchange of phonons across graphene-metal interface. Hence, the improved metal contacts to graphene not only improves the device performance, but also improves its robustness towards breakdown.

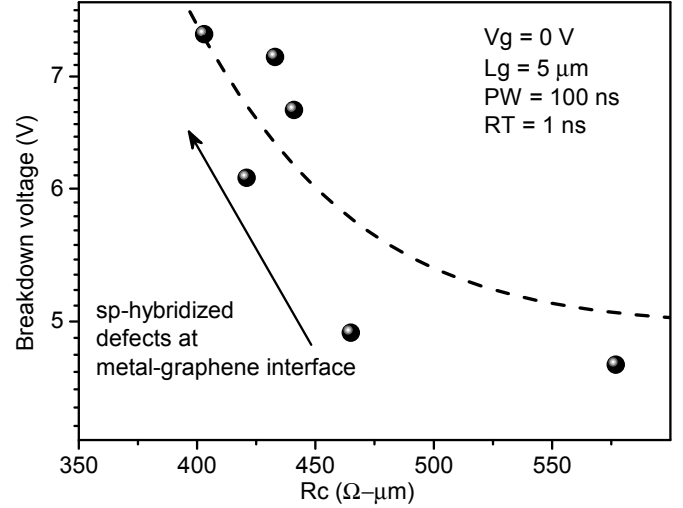


Fig. 9: Dependence of breakdown voltage on contact resistance. Devices demonstrate a down-scaling of breakdown voltage with increasing contact resistance. Engineering the contacts by creating *sp*-defects improves the metal-graphene bonding, which eventually reduces the resistive heating at contacts and increases the breakdown voltage.

V. CONCLUSION

In summary, the temporal evolution of defects and degradation due to stressing with low-electric fields has been discussed. Due to different rate of oxidation of various intrinsic defects in graphene, the time-dependent failure was found to dictate graphene's failure even under low electric-fields, which precludes the existence of critical field or critical temperature for failure. The time-dependent and field-mediated damage were explored by using integrated on-the-fly micro-Raman spectroscopy setup to capture the evolution of defects, with time and electric-field, in graphene channel under stress. Due to the absence of critical field or temperature for failure, time dependent failure of graphene, which is based on activation energies of defects, is required for the graphene failure investigations. The findings further highlight the requirement of engineered metal-graphene interface for efficient heat removal, which, in turn, was found to improve the critical field for failure.

VI. ACKNOWLEDGEMENTS

Authors would like to acknowledge Department of Science and Technology and DRDO, Govt. of India, for financial support.

REFERENCES

- [1] A. Meersha, H. B. Variar, K. Bhardwaj, A. Mishra, S. Raghavan, N. Bhat, and M. Shrivastava, "Record low metal - (CVD) graphene contact resistance using atomic orbital overlap engineering," in *2016 IEEE International Electron Devices Meeting (IEDM)*, Dec 2016, pp. 5.3.1–5.3.4.
- [2] I. Imperiale, S. Bonsignore, A. Gnudi, E. Gnani, S. Reggiani, and G. Baccarani, "Computational study of graphene nanoribbon fets for rf applications," in *2010 International Electron Devices Meeting*, Dec 2010, pp. 32.3.1–32.3.4.
- [3] G. Fiori and G. Iannaccone, "Insights on radio frequency bilayer graphene fets," in *2012 International Electron Devices Meeting*, Dec 2012, pp. 17.3.1–17.3.4.
- [4] N. C. Wang, S. Sinha, B. Cline, C. D. English, G. Yeric, and E. Pop, "Replacing copper interconnects with graphene at a 7-nm node," in *2017 IEEE International Interconnect Technology Conference (IITC)*, May 2017, pp. 1–3.
- [5] N. K. Kranthi, A. Mishra, A. Meersha, and M. Shrivastava, "Esd behavior of large area cvd graphene rf transistors: Physical insights and technology implications," in *2017 IEEE International Reliability Physics Symposium (IRPS)*, April 2017, pp. 3F–1.1–3F–1.6.
- [6] N. K. Kranthi, A. Mishra, A. Meersha, H. B. Variar, and M. Shrivastava, "Defect-assisted safe operating area limits and high current failure in graphene fets," in *2018 IEEE International Reliability Physics Symposium (IRPS)*, March 2018, pp. 3E.1–1–3E.1–5.
- [7] V. Vashchenko and V. Sinkevitch, *Physical Limitations of Semiconductor Devices*. Springer US, 2008.
- [8] L. G. Caçado, A. Jorio, E. H. M. Ferreira, F. Stavale, C. A. Achete, R. B. Capaz, M. V. O. Moutinho, A. Lombardo, T. S. Kulmala, and A. C. Ferrari, "Quantifying defects in graphene via raman spectroscopy at different excitation energies," *Nano Letters*, vol. 11, no. 8, pp. 3190–3196, Aug 2011. [Online]. Available: <https://doi.org/10.1021/nl201432g>
- [9] M. Shrivastava, N. Kulshrestha, and H. Gossner, "Esd investigations of multiwalled carbon nanotubes," *IEEE Transactions on Device and Materials Reliability*, vol. 14, no. 1, pp. 555–563, March 2014.
- [10] K. L. Grosse, V. E. Dorgan, D. Estrada, J. D. Wood, I. Vlassiok, G. Eres, J. W. Lyding, W. P. King, and E. Pop, "Direct observation of resistive heating at graphene wrinkles and grain boundaries," *Applied Physics Letters*, vol. 105, no. 14, p. 143109, 2014. [Online]. Available: <https://doi.org/10.1063/1.4896676>
- [11] D.-H. Chae, B. Krauss, K. von Klitzing, and J. H. Smet, "Hot phonons in an electrically biased graphene constriction," *Nano Letters*, vol. 10, no. 2, pp. 466–471, 2010, pMID: 20041665. [Online]. Available: <https://doi.org/10.1021/nl903167f>
- [12] S. Singha Roy, N. S. Safron, M.-Y. Wu, and M. S. Arnold, "Evolution, kinetics, energetics, and environmental factors of graphene degradation on silicon dioxide," *Nanoscale*, vol. 7, pp. 6093–6103, 2015. [Online]. Available: <http://dx.doi.org/10.1039/C4NR07531E>
- [13] M.-H. Bae, S. Islam, V. E. Dorgan, and E. Pop, "Scaling of high-field transport and localized heating in graphene transistors," *ACS Nano*, vol. 5, no. 10, pp. 7936–7944, 2011, pMID: 21913673. [Online]. Available: <https://doi.org/10.1021/nn202239y>
- [14] K. L. Grosse, M.-H. Bae, F. Lian, E. Pop, and W. P. King, "Nanoscale joule heating, peltier cooling and current crowding at graphene-metal contacts," *Nature Nanotechnology*, vol. 6, pp. 287 EP –, Apr 2011. [Online]. Available: <https://doi.org/10.1038/nnano.2011.39>

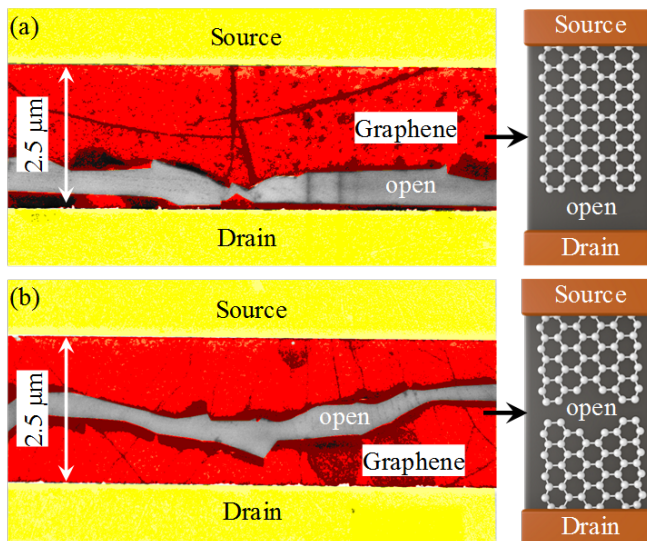


Fig. 10: Post-breakdown false-color SEM images of graphene FETs. (a) Breakdown towards the hot-contact (drain), primarily due to current crowding at the hot contact and consequent bottleneck for transfer of thermal energy from channel to contacts. (b) Breakdown away from the contacts. Efficient metal-graphene interface improves the conduction of heat from channel to metal contacts, which, in turn, shifts the location of breakdown away from the contacts. [Color coding in (a) and (b) – Red: graphene channel, Grey: Substrate and Yellow: Contacts.]